*Electronic Materials Letters, Vol. 2, No. 3 (2006), pp. 195-200*

# Nanocarving Process: Selective and Anisotropic Gas Phase Etching of Bulk $TiO_2$ Crystal into Oriented Arrays of Nanofibers

**Sehoon Yoo***

School of Materials Science and Engineering, Georgia Institute of Technology,
771 Ferst Dr. Atlanta GA 30332, USA

A simple, inexpensive gas phase reaction termed as "nanocarving process" converts $TiO_2$ grains into arrays of single crystal nanofibers by selective and anisotropic etching. This process is conducted by exposing dense polycrystalline $TiO_2$ to a hydrogen-bearing environment. This article reviews the syntheses, properties, and kinetic mechanisms of $TiO_2$ nanofibers via nanocarving process.

**Key words:** $TiO_2$, $H_2$, etching, nanofibers, nanowires, nanomaterials.

## 1. INTRODUCTION

Titanium oxide($TiO_2$) is an important engineering material that is widely used in chemical sensors[1,2], photocatalysts[3,4], dye-sensitized solar cells[5], biosensors[6], biocompatible materials[7], and Li-based batteries[8]. Since the key chemical processes associated with such devices occur at $TiO_2$ surfaces, the surface morphology of the $TiO_2$ is a key device characteristic. Especially for chemical sensing and photocatalytic applications, the high gas/solid interfacial areas associated with nanostructured oxide surfaces provide a significantly larger concentration of active sites for gas-solid interactions, which, in turn, results in enhanced catalytic activity and chemical sensitivity[9]. Numerous approaches have been explored for tailoring the surface morphology of $TiO_2$[10-12]. However, the widespread utilization of these processes is complicated by the conflicting demands for precise control of fine, well-ordered surface features and for low-cost, rapid mass production. Novel methods for fabricating well-organized oxide nano-structures that are simple and that can be readily scaled up are needed to allow for large scale, cost-effective manufacturing.

Recently, Yoo *et al*.[13] developed "nanocarving" process, which is a novel, low cost method for generating $TiO_2$ surfaces containing arrays of nanofibers. The process utilizes simple and highly scalable method involving gas phase reaction with non-combustible $H_2/N_2$ gas. Therefore, it provides *i*) precise control of fine, well-ordered surface features and *ii*) low-cost, rapid mass production. Unlike other approaches that have relied upon deposition and growth (i.e., additive processes) to synthesize one-dimensional nanostructures[14-16], the $TiO_2$ nanofibers generated by the nanocarving technique result from the anisotropic etching of $TiO_2$ grains (i.e., a subtractive process). This process yields oriented arrays of single crystal nanofibers over the exposed $TiO_2$ surfaces. The objective of the present paper is to review the syntheses, properties, and kinetic mechanisms of $TiO_2$ nanofibers via nanocarving process.

*Corresponding author: sehoon.yoo@mse.gatech.edu

## 2. TITANIUM OXIDE NANOFIBERS VIA NANOCARVING PROCESS

Dense, polycrystalline $TiO_2$ disks were used as the external surface for nanofiber formation. The disks were prepared by sintering titanium oxide powder compacts for 6 h at 1200°C in air. Secondary electron microscope (SEM) image of the surfaces of the polycrystalline $TiO_2$ disk specimen is shown in Fig. 1(a). This image reveals distinct facets on, and distinct boundaries between, the rutile grains. The dense rutile disks were then exposed to a flowing 5% $H_2$/95% $N_2$ gas mixture at 700 $^oC$ for 8 h. SEM image of the external surface of a $TiO_2$ specimen after this $H_2/N_2$ treatment is shown in Fig. 1(b). Fine fibers, with diameters of 15-50 nm were observed to have formed on the external specimen surface. Such nanofibers were organized into aligned arrays. The nanofibers formed only on the surface (Fig. 1(c)). The depth of the nanofiber region was about 1 μm for $H_2/N_2$ treatment at 700 $^oC$ for 8 hrs. Since the average grain size was 2.7 μm ($TiO_2$ sintered at 1200 $^oC$ for 6 hr), roughly half of the surface grains had transformed into nanofibers (assuming that the nanofibers formed parallel to the surface

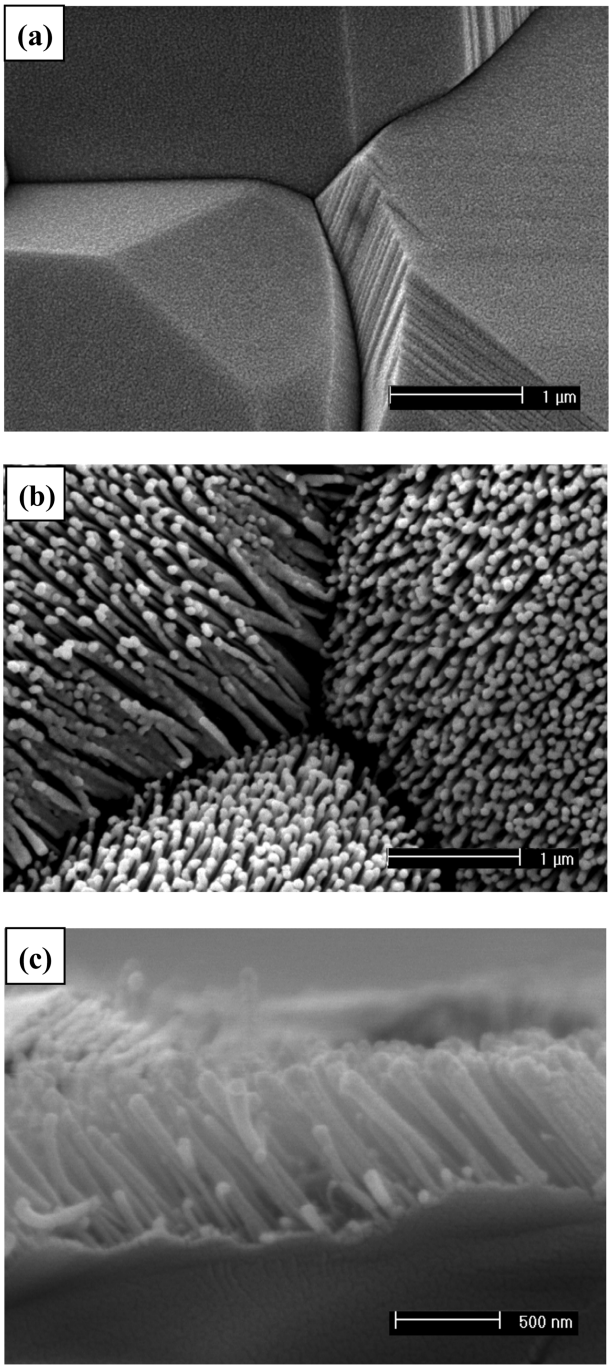


**Fig. 1.** Scanning electron micrographs of a $TiO_2$ disk surface; (a) before and (b) after $H_2/N_2$ heat treatment at 700 °C for 8 hrs. Cross-sectional SEM micrograph of nanofibers formed on the $TiO_2$ disk surface is shown in (c).

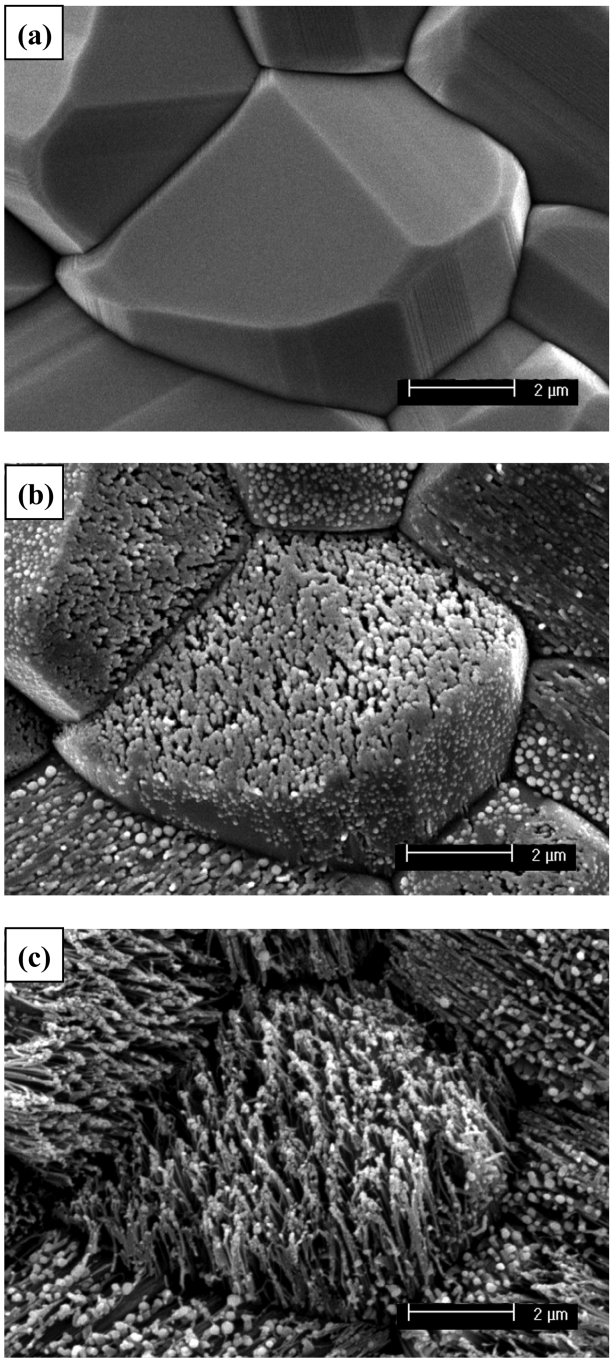


**Fig. 2.** Time sequential SEM observation of a $TiO_2$ grain during $H_2$ heat treatment. (a) before $H_2$ heat treatment, (b) after 10 min, and (c) after 8 hrs.

normal).

Despite the nanocarving occurred under reducing environment with hydrogen, the phase of the nanofibers, which were analyzed with XRD, XPS, and electron diffraction (ED), was rutile polymorph of $TiO_2$[13, 17]; that is, such hydrogen gas reaction with titanium oxide surface didn't result in transformation into distinguishably different titanium oxide phase (e.g. $Ti_3O_5$, $Ti_2O_3$, TiO, etc). The phase of the nanofibers was also consistent with what was anticipated based on the thermodynamic phase stability diagram reported in[18]. Since the temperature of nanocarving is 700 °C (973 K) and the oxygen partial pressure measured by a commercial oxygen sensor was $3 \times 10^{-22}$, the stable phase was $TiO_2$ according

to the phase stability diagram.

The $TiO_2$ nanofibers were formed by selective gas-phase etching of the $TiO_2$ along preferred crystallographic directions. Figure 2 shows SEM images that were obtained from the same $TiO_2$ grains before and after exposure to the 5% $H_2$/95% $N_2$ gas mixture for various times. Within 10 min of exposure, fine channels had formed on certain surfaces of the $TiO_2$ grains (Fig. 2(b)). After prolonged exposure (8 h), these channels had increased in depth and had become interconnected, so that discrete, aligned nanofibers were generated from a given $TiO_2$ grain (Fig. 2(c)). The overall size and shape of each aligned nanofiber array were similar to those of the starting $TiO_2$ grain from which the array was derived. These observations clearly indicated that the formation of the aligned nanofiber arrays was the result of an etching process (not a deposition process) that was selective with respect to the crystallography of $TiO_2$.

The etching process could also be tracked by thermogravimetric analysis (TGA). TGA analyses indicated that the $TiO_2$ specimens underwent a weight loss of 0.15 mg/cm$^2$ after nanocarving. Therefore, the weight decrease strongly indicated that the nanofiber formation was caused by an etching process, and not by deposition. This etching was selective and anisotropic, which led to aligned arrays of nanofibers.

## 3. IMPURITY SEGREGATION AND NANOCARVING

To identify surface impurities, x-ray photoelectron spectroscopy (XPS) was conducted on samples before- and after nanocarving. Figure 3 shows XPS survey peaks before and after nanocarving. Both samples (Fig. 3(a) and (b)) exhibited Al, Si, Ni, C peaks as well as Ti and O peaks. Fe was not detected before nanocarving (Fig. 3(a)), but it was found after nanocarving (Fig. 3(b)), which suggested that Fe segregated during nanocarving.

A transmission electron microscope (TEM) image of nanofibers and nanoparticles is shown in Fig. 4(a). Many nanoparticles with nanofibers were observed in the TEM image. Energy disperse x-ray spectroscope (EDS) analyses of the nanofiber and the nanoparticle (Fig. 4(b)) indicated that these nanoparticles were enriched in Fe and Ni, relative to the $TiO_2$-based nanofibers. In addition, the nanoparticles were likely to be metallic alloys since the O peak was not observed in the EDS pattern of the nanoparticle. These nanoparticles appear to have been generated during the $H_2/N_2$ gas treatment by the external reduction of the Fe and Ni oxides present as impurities in the starting $TiO_2$ powder.

Figure 5 shows SEM micrographs of $TiO_2$ grains after nanocarving. In Fig. 5, only half of the grain transformed into nanofibers and the region where no fiber was generated had nanoparticles with the diameter of few tenths of nanom-

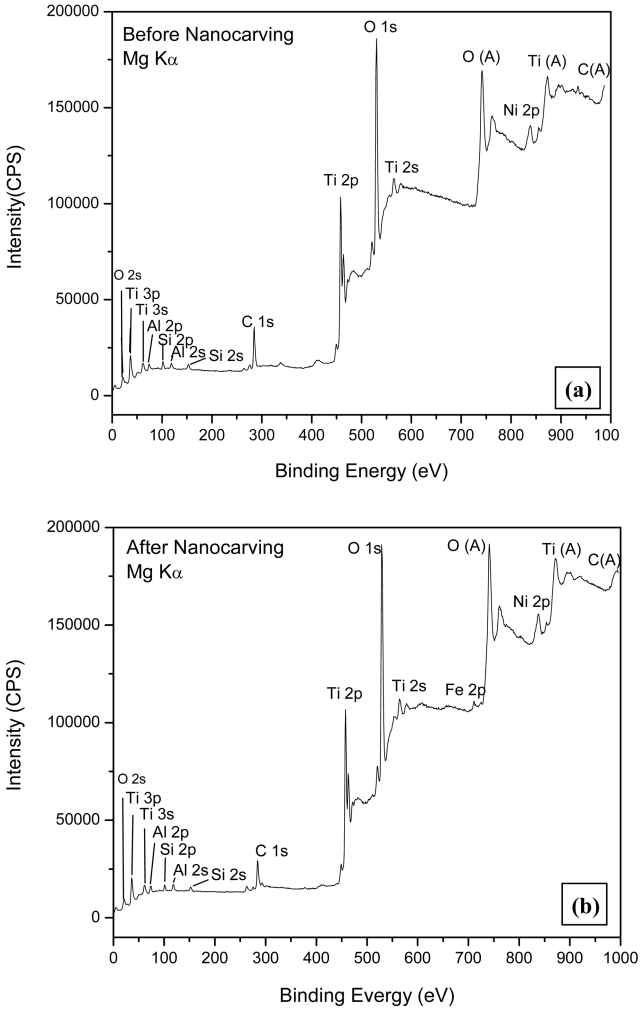


**Fig. 3.** Survey curves from x-ray photoelectron spectroscopy (XPS) of a $TiO_2$ specimen (a) before and (b) after nanocarving.

eters. In addition, the end tips of nanofibers were round and possessed similar diameters as the nanoparticles, i.e. the nanoparticles were sitting on the end tips of nanofibers. Since TEM sample preparation utilized ultrasonic energy to remove nanofibers from $TiO_2$ disk surfaces, the ultrasonic energy may have also separated the nanoparticles from the end tips of nanofibers. Hence, isolated nanoparticles in Fig. 4 were come from the end tips of nanofibers. Gazzoli *et al.* observed Fe segregation on the surface of Fe-doped (up to 8 %) $TiO_2$ via $H_2$ reduction and reported that near the segregated Fe particles in contact with $TiO_2$, a strong metal-semiconductor interaction (SMSI) occurred, causing a reduction of the nearby $TiO_2$ matrix[19]. In our system, the segregated Fe-Ni alloy particles, which exhibit SMSI with $TiO_2$, may act as catalysts to enhance the reduction of $TiO_2$ near the segregated particles. Hence, the selective etching for nanofiber formation was appeared to be caused by reduction of $TiO_2$ matrix near the segregated particles.

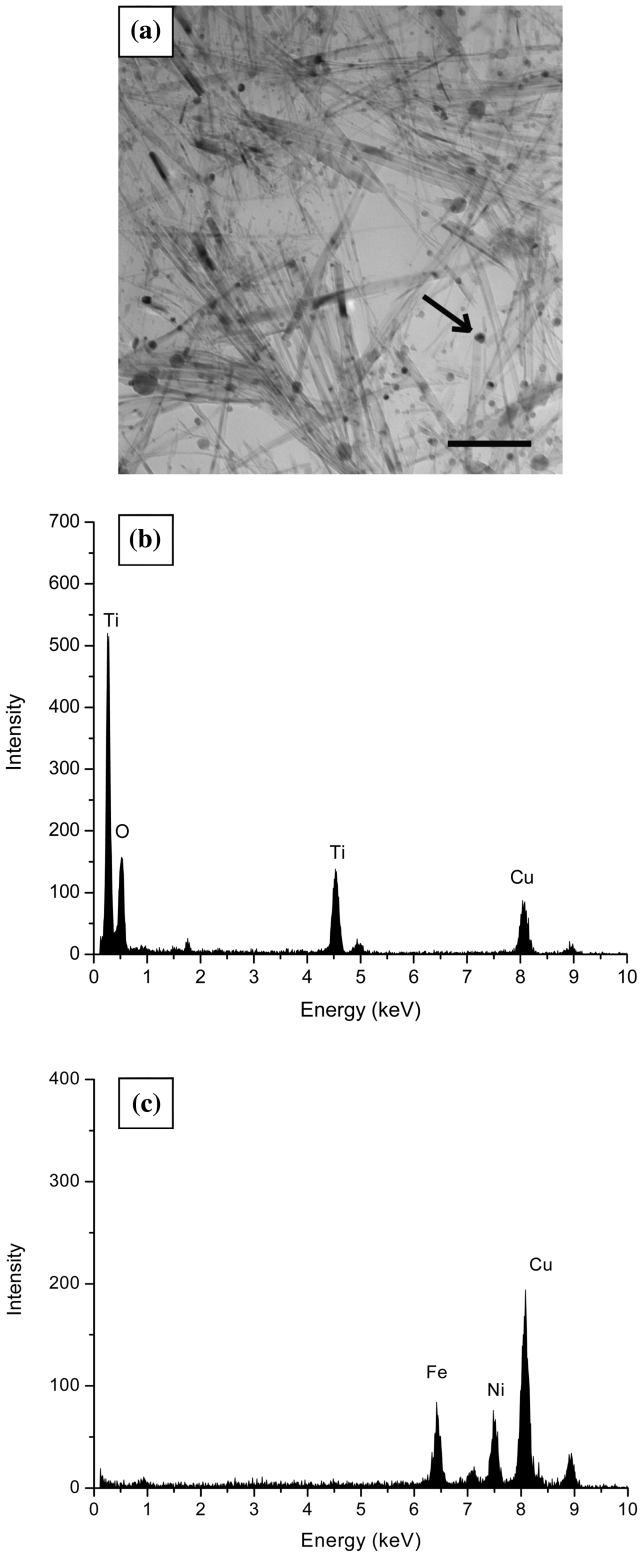


**Fig. 4.** (a) TEM image of several nanofibers with nanoparticles (one nanoparticle is indicated by the arrow). Scale bar, 200 nm. (b) Energy dispersive x-ray spectroscopy (EDS) analyses of a nanofiber. (c) EDS analyses of a nanoparticle (note: Cu peaks were generated by the carbon-coated copper grid used to support the sample).

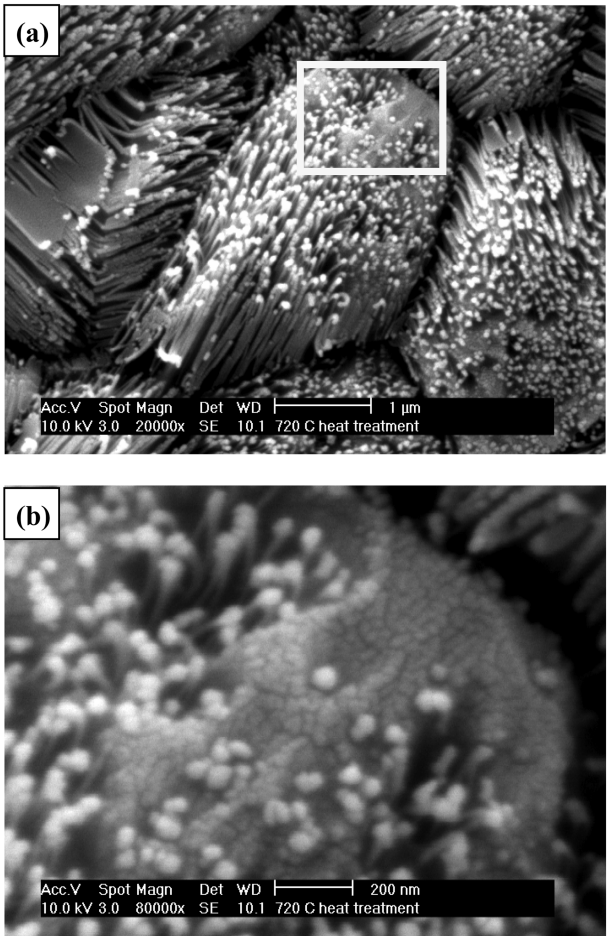


**Fig. 5.** SEM micrographs of a $TiO_2$ disk surface after $H_2/N_2$ heat treatment, showing nanofibers with nanoparticles. (a) low magnification and (b) high magnification of the area enclosed by a square in (a).

**Table 1.** Calculated Ti – O bond energy on three primary plane (110), (100) and (001)

| Surface | Oxygen atom removed from surface | Bond energy (eV) |
|---|---|---|
| (110) | First O with three Ti-O bonds | 3.02 |
| | Second O with three Ti-O bonds | 2.99 |
| (100) | First O with two Ti-O bonds | 2.12 |
| | Second O with three Ti-O bonds | / |
| (001) | First O with two Ti-O bonds | 1.24 |
| | Second O with two Ti-O bonds | 1.44 |

## 4. NANOCARVING IN PREFERRED ORIENTATION

Selective area electron diffraction (SAED) analyses on the $TiO_2$ nanofibers revealed that the long dimension (fiber axis) of each nanofiber was parallel to the <001> crystallographic direction of rutile $TiO_2$[13]. This indicated that the preferred direction of the gas phase etching was <001>. The <001>

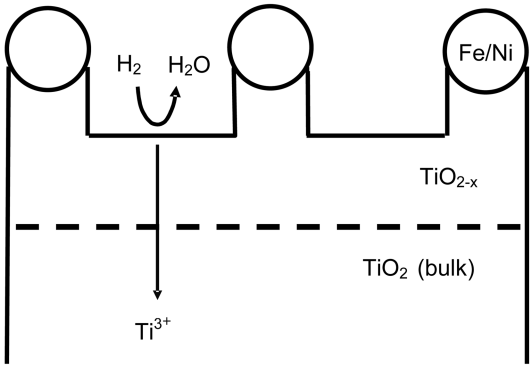


**Fig. 6.** Schematic illustration of $TiO_2$ nanocarving. Oxygen is removed from the titania surface to form water vapor during nanocarving, so as to leave behind a reduced form of titania, $TiO_{2-x}$. Remnant titanium ions diffuse away from the reacting surface towards the bulk of the polycrystalline titania specimen.

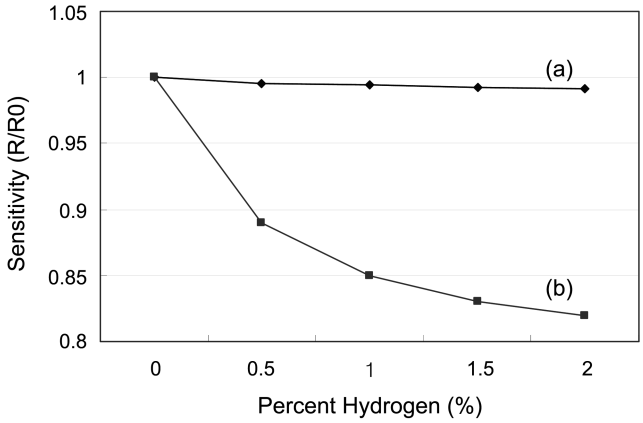


**Fig. 7.** Gas sensitivity ($R/R_0$) of $TiO_2$ disk sensors of (a) without and (b) with nanofibers when exposed to 0 to 2 % $H_2$ gas at 400°C. Background gas was 10 % $O_2$ balanced with $N_2$.

directionality or anisotropy can be explained by the bond energy between Ti−O. Ti−O bond energy on primary planes, (110), (100) and (001) was calculated and it was found out the Ti−O bond energy on the (001) plane is the lowest among three planes (Table 1). Therefore, an oxygen atom on the (001) plane was relatively easy to remove, so that preferred etching occurred along the <001> direction during the nanocarving process. This <001> anisotropy has also been observed for the photoelectrochemical (PEC) etching of $TiO_2$ single crystals[20]. Nanochannels produced by PEC etching were aligned in the <001> direction, which suggested that oxygen removal along the <001> direction was easier than from the other directions.

## 5. KINETIC MECHANISM OF NANOCARVING

The schematic of nanocarving mechanism is shown in Fig. 6. The chemical reaction of the nanocarving process is:

$$TiO_2(s) + xH_2(g) \rightarrow TiO_{2-x}(s) + xH_2O(g). \quad (1)$$

With reaction (1), oxygen is removed from the $TiO_2$ surface to form water vapor during nanocarving, so as to leave behind a reduced form of titanium oxide, $TiO_{2-x}$. To maintain the O : Ti stoichiometry on the surface close to 2.0 as oxygen leaves as $H_2O(g)$, the excess Ti ions are removed from the surface to the bulk $TiO_2$[21]. Thermogravimetric(TG) analyses upon nanocarving revealed that the reaction-induced weight loss followed a parabolic rate law, which was also consistent with a solid state diffusion-controlled process[21]. In addition, the grain boundary diffusion of Ti ions is important transport mechanism for nanocarving process[21].

## 6. GAS SENSING PERFORMANCE OF TITANIUM OXIDE NANOFIBERS

$TiO_2$ has been widely used for detecting various gas species such as $H_2$, CO, $H_2O$ and $O_2$[2, 22-25]. Recently, many researcher have focused on the use nanoscale $TiO_2$ as a gas sensor[26-30], since it has been known that nanoscale $TiO_2$ exhibits enhanced sensitivity. Li *et al.*[9] showed that the enhanced sensitivity of nanoscale $TiO_2$ was due to the large surface area. To date, most nanoscale $TiO_2$ for gas sensors has been in the form of granular/particulate type nanomaterial. Such nanoparticles should be mounted on substrates by spin coating or screen printing. The $TiO_2$ nanofibers via nanocarving process, however, were formed on the sample surface; so no additional process was required for mounting nanomaterials on the $TiO_2$ substrate. To inspect the possibility of $TiO_2$ nanofibers as gas sensors, a sensing test of $TiO_2$ disks containing nanofibers was performed and the result is shown in Fig. 7. For comparison, a $TiO_2$ disk with no nanofiber (just sintered disks) was also tested. The test gas was $H_2$ balanced with 10% $O_2/N_2$. As shown in Fig. 7, $TiO_2$ nanofiber specimens exhibited a significant change in sensitivity upon exposure to increasing concentrations of hydrogen gas. No such decrease was detected with as-sintered $TiO_2$ specimens (i.e., in the absence of nanofiber formation). Comparing with as-sintered $TiO_2$ which showed no response, the enhanced surface area nanofiber-based sensors exhibited good sensitivity.

## 7. CONCLUSIONS

Simple gas phase reaction under different conditions creates various nanostructures of $TiO_2$. $TiO_2$ nanofibers were produced by a nanocarving process (heat treatment in $H_2/N_2$ 700 $^oC$ for 8 hrs), which is a selective and anisotropic etching technique. The phase of nanofibers was confirmed to be rutile, $TiO_2$. Fe-Ni alloy metal nanoparticles were observed on the end tip of $TiO_2$ nanofibers. The direction of the etching for $TiO_2$ nanofiber formation was <001>. Oxygen is

removed from the $TiO_2$ surface to form water vapor during nanocarving, so as to leave behind a reduced form of titania, $TiO_{2-x}$. The titanium ions at the reacting surface then diffused into the bulk of the titania specimen. Comparing with as-sintered $TiO_2$ sensors which showed no response, the nanofiber-based sensors exhibited good sensitivity.

## REFERENCES


1. L. D. Birkefeld, A. M. Azad, and S. A. Akbar, *J. Am. Ceram. Soc.* **75**, 2964 (1992).
2. P. I. Gouma, M. J. Mills, and K. H. Sandhage, *J. Am. Ceram. Soc.* **83**, 1007 (2000).
3. Y. Nakato, H. Akanuma, J.-i. Shimizu, and Y. Magari, *J. Electroanal. Chem.* **396**, 35 (1995).
4. S. Matsuda and A. Kato, *Appl. Catal.* **8**, 149 (1983).
5. B. O'Regan and M. Graetzel, *Nature* **353**, 737 (1991).
6. E. Topoglidis, A. E. G. Cass, G. Gilardi, S. Sadeghi, N. Beaumont, and J. R. Durrant, *Anal. Chem.* **70**, 5111 (1998).
7. Q. Li, G. Luo, and J. Feng, *Electroanal.* **13**, 359 (2001).
8. C. Natarajan, K. Setoguchi, and G. Nogami, *Electrochimica Acta* **43**, 3371 (1998).
9. G.-J. Li, X.-H. Zhang, and S. Kawi, *Sens. Actuator. B* **60**, 64 (1999).
10. X. Y. Zhang, L. D. Zhang, W. Chen, G. W. Meng, M. J. Zheng, L. X. Zhao, and F. Phillipp, *Chem. Mater.* **13**, 2511 (2001).
11. S. K. Pradhan, P. J. Reucroft, F. Yang, and A. Dozier, *J. Cryst. Growth* **256**, 83 (2003).
12. Z. Miao, D. Xu, J. Ouyang, G. Guo, X. Zhao, and Y. Tang, *Nano Lett.* **2**, 717 (2002).
13. S. Yoo, S. A. Akbar, and K. H. Sandhage, *Adv. Mater.* **16**, 260 (2004).
14. O. K. Varghese, D. Gong, M. Paulose, C. A. Grimes, and E. C. Dickey, *J. Mater. Res.* **18**, 156 (2003).
15. D. Li and Y. Xia, *Nano Lett.* **3**, 555 (2003).
16. J.-J. Wu and C.-C. Yu, *J. Phys. Chem. B* **108**, 3377 (2004).
17. S. Yoo, S. A. Akbar, and K. H. Sandhage, *Ceram. Inter.* **30**, 1121 (2004).
18. D. C. Lynch and D. E. Bullard, *Metall. Mater. Trans. B* **28B**, 447 (1997).
19. D. Gazzoli, G. Minelli, and M. Valigi, *Mater. Chem. Phys.* **21**, 93 (1989).
20. A. Tsujiko, T. Kisumi, Y. Magari, K. Murakoshi, and Y. Nakato, *J. Phys. Chem. B* **104**, 4873 (2000).
21. S. Yoo, S. A. Dregia, S. A. Akbar, H. Rick, and K. H. Sandhage, *J. Mater. Res.* **21**, 1822 (2006).
22. R. K. Sharma, M. C. Bhatnagar, and G. L. Sharma, *Sens. Actuator. B* **45**, 209 (1997).
23. N. O. Savage, S. A. Akbar, and P. K. Dutta, *Sens. Actuator. B* **72**, 239 (2001).
24. Y. Li, W. Wlodarski, K. Galatsis, S. H. Moslih, J. Cole, S. Russo, and N. Rockelmann, *Sens. Actuator. B* **83**, 160 (2002).
25. M. L. Frank, M. D. Fulkerson, B. R. Patton, and P. K. Dutta, *Sens. Actuator. B.* **87**, 471 (2002).
26. Y. Zhu, J. Shi, Z. Zhang, C. Zhang, and X. Zhang, *Anal. Chem.* **74**, 120 (2002).
27. A. M. Taurino, M. Epifani, T. Toccoli, S. Iannotta, and P. Siciliano, *Thin Solid Films* **436**, 52 (2003).
28. O. K. Tan, W. Cao, W. Zhu, J. W. Chai, and J. S. Pan, *Sens. Actuator. B* **93**, 396 (2003).
29. I. Kosacki and H. U. Anderson, *Sens. Actuator. B* **48**, 263 (1998).
30. N. Bonini, M. C. Carotta, A. Chiorino, V. Guidi, C. Malagu, G. Martinelli, L. Paglialonga, and M. Sacerdoti, *Sens. Actuator. B* **68**, 274 (2000).